On-Chip Topological Multichannel Filtering and Routing Device Based on Synthetic Dimension

Zhihao Feng [ID], Hongyi Yuan [ID], Hongyu Zhang, and Yuefeng Zhao [ID]

Abstract—On-chip topological nanophotonic filtering and routing devices are important components of integrated nanophotonic chip. The device filters topological photonic states with multiple frequencies and routes them into different output ports, respectively. However, there is no effective method to implement such devices to date. Here, an on-chip topological five-channel filtering and routing device is realized for the first time. Topological edge states are constructed based on synthetic dimension, which can use dielectric materials to construct topological photonic states without external magnetic field. This method has advantages including simple structure, easy integration, and high signal-to-noise ratio. The implementation of on-chip topological multichannel filtering and routing device is of great significance to the development of topological nanophotonic devices.

Index Terms—Filter, router, photonic crystal, topological edge state.

I. INTRODUCTION

TOPOLOGICAL nanophotonic devices are robust due to the topological protection, so the disorder and deletion of the structure bring little influence on the performance of nanophotonic devices [1], [2]. In the design of on-chip topological nanophotonic devices, frequency, as a basic degree of freedom of light, plays an important role as information carrier. Recently, there have been some typical frequency related topological photonic devices, such as topological filters [3], [4], topological rainbow devices [5], [6], [7], [8], and topological routers [9]. Among these devices, the topological nanophotonic filter is a frequency-selective device that allows multiple specific frequencies of incident light to pass while filtering out other frequencies. However, the filtered light with frequencies selection generally cannot be separated in space, which means that they are all output from the same channel. This limits the application of topological nanophotonic filters in integrated nanophotonic chips. When

solving the problem of separating light of different frequencies, we can use nanophotonic routers to guide signals of different frequencies into different ports for output [10], [11], [12], [13], [14], so the realization of on-chip topological nanophotonic filtering and routing devices are of great significance. However, there are few reports on topological multichannel filtering and routing device. It is a challenging task to realize on-chip filter and router in topological nanophotonics.

Topological edge states based on all-dielectric materials have the advantages of no external magnetic field and easy on-chip integration. For example, topological photonic states can be constructed by deforming a honeycomb lattice of cylinder hexagons using all-dielectric materials [15]. Topological edge states can also be constructed using valley photonic crystals [16], [17], [18], [19]. In recent studies, topological edge states are constructed by introducing an extra degree of freedom in the photonic system, called the synthetic dimension [20], [21], [22]. In two-dimensional all-dielectric photonic crystals, the translational degrees of freedom of the photonic crystal structure can be used as the synthetic dimension for constructing topological edge states without limitations for lattice types [5]. The topological edge states can be regulated by adjusting the synthesis dimension so that the device can have various functions on the premise of simple structure. The topological photonic states based synthetic dimension provides effective method for the construction of on-chip nanophotonic topological devices [7].

In this work, we realize an on-chip topological multichannel filtering and routing device based on synthetic dimension. The function of filtering is realized by introducing displacement parameter as synthetic dimension to construct topological photonic waveguides. The waveguides allow only guiding modes to be transmitted forward, while other modes are filtered out. The integrated routing function is realized by the combination of multiple waveguides with different displacement parameters. Therefore, the guiding modes with different frequencies can be transmitted forward into different waveguides and output at corresponding ports. The device can route the target frequency to the specified port distinctly and greatly suppress the noise of other frequencies. The device based on synthetic dimension provides a new approach for the application of topological photonics in nanophotonic devices.

Zhihao Feng and Yuefeng Zhao are with the Shandong Provincial Engineering and Technical Center of Light Manipulations and Shandong Provincial Key Laboratory of Optics and Photonic Device, School of Physics and Electronics, Shandong Normal University, Jinan 250358, China (e-mail: 17861401017@163.com; yuefengzhao@sdnu.edu.cn).

Hongyi Yuan and Hongyu Zhang are with the Beijing Key Laboratory of Nanophotonics and Ultrafine Optoelectronic Systems, School of Physics, Beijing Institute of Technology, Beijing 100081, China (e-mail: 2584557325@qq.com; 3120215775@bit.edu.cn).

II. METHOD OF CONSTRUCTING TOPOLOGICAL EDGE STATE

The device is based on all-dielectric photonic crystals composed of a square lattice of dielectric cylinders embedded in
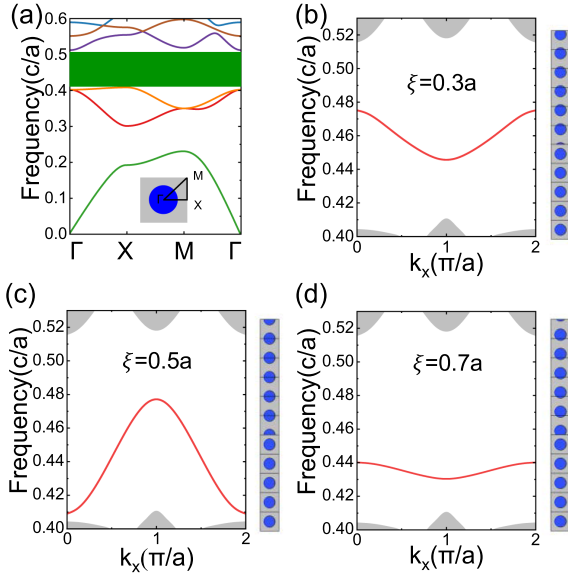
Fig. 1. (a) Dispersion relations of the unit cell of the photonic crystal. The lattice constant of the square lattice is a. The gray square represents air. (b)–(d) Topological edge states of different displacement parameters. The gray regions are bulk bands. The structure of supercells is shown on the right side.

air. The bulk dispersion of the transverse magnetic (TM) modes is shown in Fig. 1(a). The lattice constant is a, the radius of the dielectric cylinder is $0.3a$ and the material of the dielectric cylinders is silicon. The reason why $0.3a$ is chosen as the radius of the cylinders is because the wider bandgap width at this point facilitates the device design. The displacement parameter ξ is introduced as the synthesis dimension on the dielectric cylinders. It forms a 3D space of (k_x, k_y, ξ) with k_x and k_y in the momentum space of the photonic crystal. When k_y is fixed, the Zak phase $\theta_n^{(Zak)}(k_y, \xi)$ corresponding to parameters (k_y, ξ) and band n is defined as:

$$\theta_n^{(Zak)}(k_y, \xi) = \int_{-\frac{\pi}{a}}^{\frac{\pi}{a}} \langle u_n(k_x, k_y, \xi) \left| i\frac{\partial}{\partial k_x} \right| u_n(k_x, k_y, \xi) \rangle dk_x. \tag{1}$$

$|u_n(k_x, k_y, \xi)\rangle$ is the periodic part of the Bloch state of nth band with parameter (k_x, k_y, ξ). For a fixed k_y, as ξ varies from $-a/2$ to $a/2$ the Chern number $C_n(k_y)$ of the band n and parameter k_y is obtained by dividing the Zak phase winding by 2π:

$$C_n(k_y) = \frac{1}{2\pi} \int_{-\frac{a}{2}}^{\frac{a}{2}} \partial_\xi \theta_n^{(Zak)}(k_y, \xi) d\xi. \tag{2}$$

Here, when ξ changes by a period, the Zak phase changes by 2π, and the Chern number of each isolated band is equal to 1 if there is one band below the gap, which corresponds to the one topological photonic state at the interface [5], [23]. The sum of Chern numbers of the band below the gap is the total Chern number characterizing a gap. Therefore, the topological edge states are generated by combining the undeformed structure with the structure with displacement parameter. According to the bulk-edge correspondence in the translational deformation,

the Chern number difference of the system on either sides of the interface is the number of topological edge states in one direction. In other words, during the translation of ξ, n modes always raise their energies out of the nth bulk energy band and go across the band gap between the nth and $(n + 1)$th bands [24].

We choose the green band gap in Fig. 1(a) as the operating frequency range, which is 0.412 c/a–0.517 c/a. The reason for choosing this band gap as the operating frequency range is the emergence of edge states according to the bulk–edge correspondence. When the displacement parameter ξ changes from 0 to a, three topological edge states will be generated and different ξ corresponds to different frequencies with high transmission, which is more conducive to the design of the topological multichannel filtering and routing device. Therefore, we can select different topological edge states as different outlet transmission modes according to our need. Fig. 1(b)–(d) show the topological edge states and supercell structures under different displacement parameters.

The distribution of |E| in topological photonic waveguide based on the synthetic dimension is shown in Fig. 2(a). This is calculated by the finite element method (FEM) in COMSOL Multiphysics software. The left side is the structure with the displacement parameter introduced. The displacement parameter ξ is introduced in the x-direction. When ξ changes, the relationship between the frequencies and the normalized transmission is shown in Fig. 2(b). It is clear that different ξ and different frequencies correspond to different transmissions. The three bright strips in the Fig. 2(b) correspond successively to the three topological edge states in Fig. 1(b)–(d). The third topological edge state in Fig. 2(b) is darker. This is because compared with other modes of topological edge states, it is more localized in the dielectric cylinders and is not easy to leak to air, as shown in Fig. 2(c). In the process of device design, in order to better carry out optical injection, part of the medium barrel is removed at the beginning of the interface [25].

We construct a double 90° waveguide bend to compare the difference between the topological edge states based on the synthetic dimension and the conventional photonic defect edge modes. When the incident light frequency is $0.43c/a$, the distribution of |E| is shown in Fig. 2(d). The photonic defect edge modes can still transmit but will have dispersion after bending. In order to reduce the dispersion at the bend and achieve broadband and high efficiency transmission, the structure at the bend of the waveguide should be further optimized [26], [27], [28], [29], [30]. Because the topological edge modes have the properties of topological protection, the distribution of |E| does not weaken significantly when it passes through the double 90° bends. At the same frequency, the transmission of the double-bend topological waveguide is only 0.08 less than that of the straight topological waveguide of the same length. This is because when constructing two 90° bends, there will be disturbance at the bends, which will cause small energy loss.

III. DESIGN AND ANALYSIS

We first design a topological dual-channel multi-mode filtering and routing device, as shown in Fig. 3(a). Each port
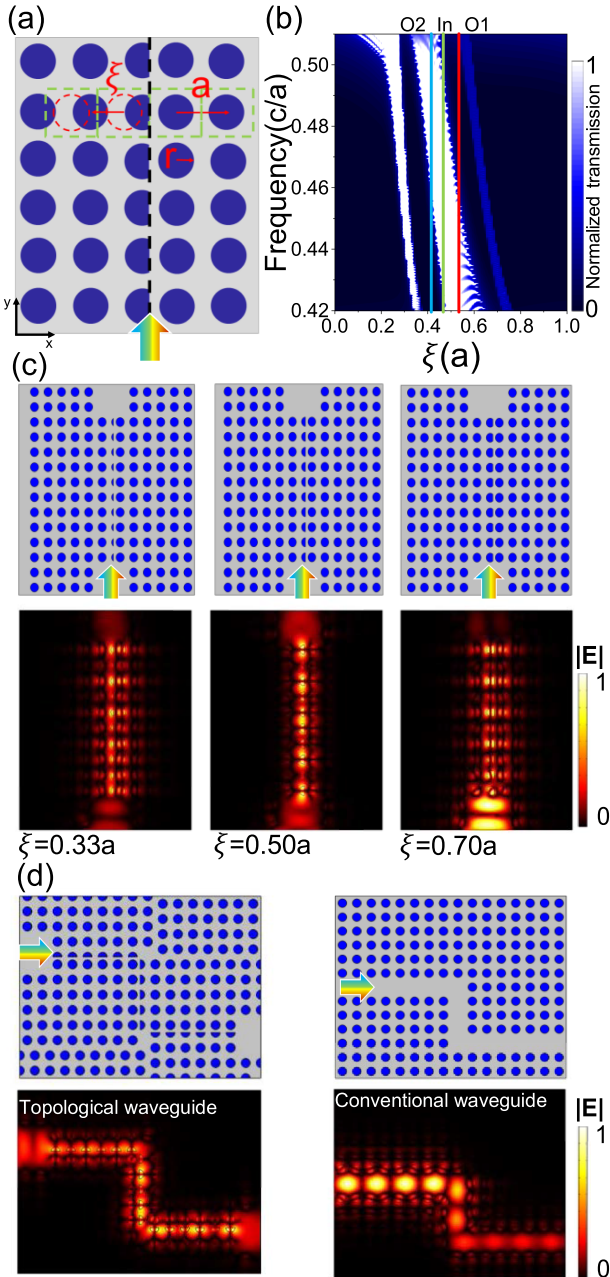
Fig. 2. (a) Topological photonic waveguide. The red dotted lines indicate the original positions of the dielectric cylinders. The colored arrow represents the incident light source. (b) The relationship between the normalized transmission and the displacement parameter ξ at different frequencies. The three lines are the displacement parameters corresponding to the three topological waveguides of the topological dual-channel filtering and routing device in Fig. 3. (c) The distribution of |E| in the topological photonic waveguides with different displacement parameters at the same frequency. Incident light frequency is 0.433 c/a. (d) The distribution of |E| in topological waveguides and conventional waveguides at the same frequency.
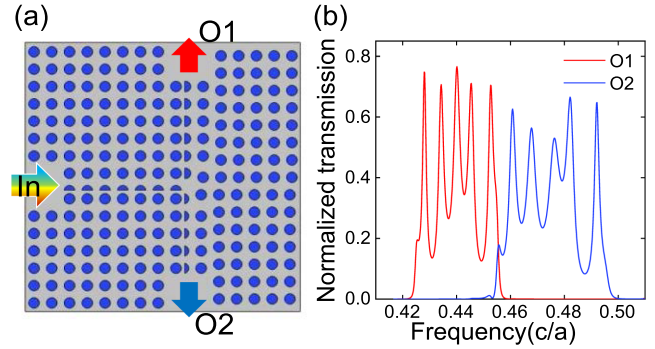

Fig. 3. (a) Topological dual-channel filtering and routing device structure. (b) The normalized transmission of different ports in the incident light frequency range of 0.42 c/a–0.50 c/a.

can support five output modes, with little overlap between the two ports' output modes, as shown in Fig. 3(b). The reason for realizing multimode output is that the device has the properties of photonic crystal waveguide resonator due to its structure, which can be considered as a Fabry-Perot cavity [31], [32]. When the displacement parameter is fixed, the number of output modes

increases as the waveguide becomes longer. So the number and frequency of output modes can be controlled by adjusting the displacement parameters and waveguide length. The displacement parameter of the left topological bus waveguide is 0.467a, allowing the optical output with frequencies between 0.42 c/a and 0.50 c/a. The displacement parameter of the O1 output topological waveguide is 0.533a, allowing five modes of output in low frequency domain. The displacement parameter of the O2 outlet topological waveguide is 0.421a, allowing five modes output in the high frequency domain. The center frequencies of light output from O1 are 0.428 c/a, 0.434 c/a, 0.440 c/a, 0.440 c/a, and 0.452 c/a. The center frequencies of light output from O2 are 0.460 c/a, 0.467 c/a, 0.476 c/a, 0.482 c/a, and 0.492 c/a.

On the basis of the dual-channel multi-mode filtering and routing device, we introduce more topological waveguides with different displacement parameters and finally realize the topological five-channel filtering and routing device as shown in Fig. 4(a). It consists of nine topological photonic waveguides with different displacement parameters, including one bus waveguide, five output waveguides, and three waveguides located inside the structure for primary filtering and routing of light. This device can output light of five different frequencies in the frequency range of 0.42 c/a–0.51 c/a from five ports.

A topological waveguide with a displacement parameter of 0.46a is used as the bus waveguide on the left, so that it can allow all modes in the frequency range from 0.42 c/a to 0.51 c/a to pass.

The incident light is then divided into three parts and transmitted in three directions. The light with frequencies lower than 0.45 c/a will go down into the waveguide with a displacement parameter of 0.32a. Light with frequencies above 0.47 c/a will go up into the waveguide with a displacement parameter of 0.26a. The light with frequencies between 0.45 c/a and 0.47 c/a will enter the right topological waveguide with displacement parameters of 0.64a for the first half and 0.62a for the second half. The reason why this combination is used in the right waveguide is to obtain a single-mode output from O3 with a center frequency of 0.465 c/a. After the initial filtering and routing, the guiding modes will enter the output waveguide with different displacement parameters and output from different ports. The
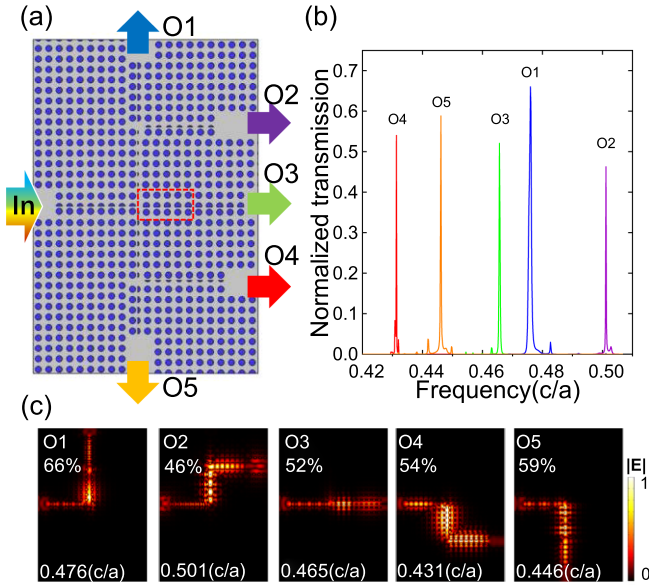
Fig. 4. (a) Topological five-channel filtering and routing device structure. (b) The normalized transmission at different outlets. (c) Normalized transmission and the distribution of |E| with different frequencies.
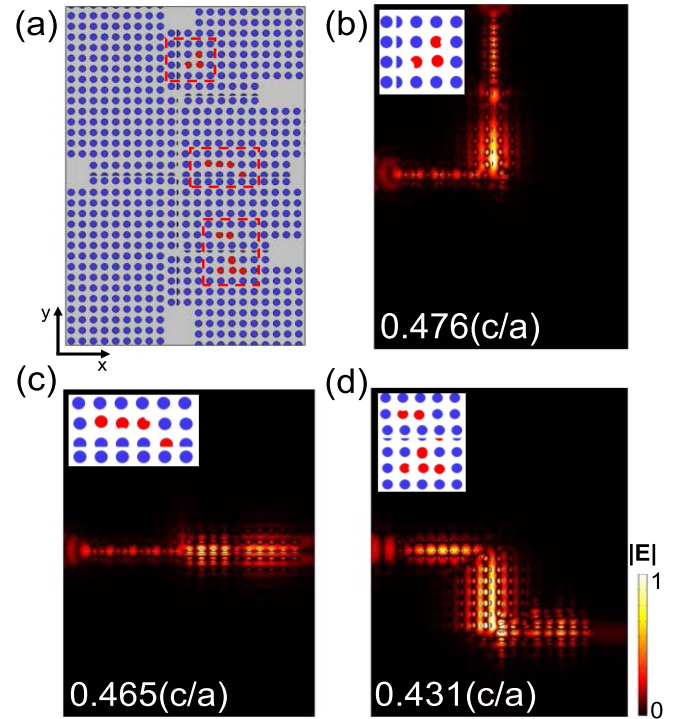

Fig. 5. (a) Structure drawing and local enlarged drawing after introducing perturbation. The structures with random perturbations are marked with red in the figure, and the perturbation ranging from 0.03a to 0.09a is randomly introduced in the x and y directions. (b)–(d) The distribution of |E| with different frequencies.

displacement parameters of O1, O2, O4, and O5 output topological photonic waveguides are $0.492a$, $0.354a$, $0.345a$, and $0.437a$, respectively. Their final output center frequencies are $0.476\,c/a$, $0.501\,c/a$, $0.431\,c/a$, and $0.446\,c/a$. Fig. 4(b) shows the normalized transmission of different ports within the frequency range of incident light from $0.42\,c/a$ to $0.51\,c/a$.

It can be seen that the topological five-channel filtering and routing device has excellent filtering and routing functions, and there is no signal overlap between different output frequencies. In addition, the output modes of different ports can be adjusted by changing the displacement parameters or the combination of topological photonic waveguides. Due to the robustness of the topological device, even if there is structural offset and 90-degree bending at the joint, the device still has good performance. Fig. 4(c) shows the center frequencies of the output light, the distribution of |E| and normalized transmission when incident light is in the frequency range of $0.42\,c/a$–$0.51\,c/a$.

The signal-to-noise ratio (SNR) is calculated by using the formula $10\log(S/N_n)$, where S is the signal strength on the target output port, and N_n is the signal strength on the other ports [33]. Because the transmission is calculated by the ratio of the output signal strength to the input signal strength, and the input signal strength is the same at different frequencies, the ratio of transmission between output ports is equal to the ratio of output signal strength, so we use the transmission to calculate the SNR. At the same frequency, the transmission on the objective output port is regarded as signal, and the transmission on the other output port is regarded as noise. The results are shown in Table I. It can be seen that the device has high SNR, which proves that the device has good filtering and routing performance. In addition, topological filtering and routing devices with any channel number can be implemented as long as there is a suitable topological waveguide structure and a sufficiently wide band

gap. The increase of the channel number is more conducive to the improvement of information transmission capacity.

In addition to the energy loss caused by the 90° bends, the reason for the loss of energy in the whole device may be more complicated after introducing different displacement parameters. For example, to make the noise strength of other channels is close to zero by adjust the topological waveguide displacement parameter, which leads to a reduction in signal strength as well. Although the transmission is reduced, it has a higher SNR. Therefore, if we want to improve the transmission further, we can optimize the structure of the bend to reduce the

TABLE I
THE SIGNAL-TO-NOISE RATIO OF THE OUTPUT FREQUENCIES

	O1 0.476(c/a)	O2 0.501(c/a)	O3 0.465(c/a)	O4 0.431(c/a)	O5 0.446(c/a)
O1	------	24.68dB	38.90dB	72.51dB	79.96dB
O2	64.85dB	------	52.27dB	84.24dB	123.68dB
O3	54.60dB	32.94dB	------	54.46dB	71.61dB
O4	98.34dB	65.73dB	44.70dB	------	69.48dB
O5	55.95dB	51.59dB	62.12dB	34.06dB	-------

disorder at the bend. We can also optimize the combination of topological waveguides with different displacement parameters.

In order to study the robustness of the topological multi-channel filtering and routing device, we randomly select three waveguides to introduce some perturbation. The introduced perturbations consist of displacing and deforming the dielectric cylinder, as shown in Fig. 5(a). The introduction of random disturbance in the device breaks the periodicity of the lattice, but the distribution of |E| indicates that the device can still work normally, as shown in Fig. 5(b)–(d). It is found that there is nearly no any backscattering when the light reaches the disordered region, which proves the robustness of the device.

IV. CONCLUSION

In conclusion, we have realized on-chip topological multichannel filtering and routing devices based on synthetic dimension using dielectric materials. A topological dual-channel multi-mode filtering and routing device is designed first based on the principle of synthetic dimension, realizing that each outlet can output five modes. The capacity of optical communication information transmission can be further expanded when the number of channels is increased. On this basis, we implement an on-chip topological five-channel filtering and routing device. It can filter the topological photonic states within the frequency range from $0.42c/a$ to $0.51c/a$, and then separate the light of different frequencies and output them from different ports. Due to the combination of multiple topological photonic waveguides, ultra-high signal-to-noise ratio can also be achieved, and the device has the advantages of simple structure, easy integration and robustness. Topological interface states based on synthetic dimension of photonic crystal can be easily tuned by introducing other degrees of freedom in the synthetic parameter space, which is beneficial to the design of topological photonic devices on chip. This work lays a foundation for the development of topological photonic devices.

ACKNOWLEDGMENT

REFERENCES

[1] L. Lu, J. D. Joannopoulos, and M. Soljačić, "Topological photonics," *Nature Photon.*, vol. 8, pp. 821–829, Nov. 2014.

[2] A. B. Khanikaev and G. Shvets, "Two-dimensional topological photonics," *Nature Photon.*, vol. 11, no. 12, pp. 763–773, Dec. 2017.

[3] L. Gu et al., "A topological photonic ring-resonator for on-chip channel filters," *J. Lightw. Technol.*, vol. 39, no. 15, pp. 5069–5073, Aug. 2021.

[4] Y.-C. Lin, S.-H. Chou, and W.-J. Hsueh, "Robust high-Q filter with complete transmission by conjugated topological photonic crystals," *Sci. Rep.*, vol. 10, Dec. 2020, Art. no. 7040.

[5] C. Lu, C. Wang, M. Xiao, Z. Q. Zhang, and C. T. Chan, "Topological rainbow concentrator based on synthetic dimension," *Phys. Rev. Lett.*, vol. 126, no. 11, Mar. 2021, Art. no. 113902.

[6] L. Liang, X. Zhou, J.-H. Hu, H.-X. Wang, J.-H. Jiang, and B. Hou, "Rainbow trapping based on higher-order topological corner modes," *Opt. Lett.*, vol. 47, no. 6, pp. 1454–1457, Mar. 2022.

[7] C. Lu et al., "On-chip nanophotonic topological rainbow," *Nature Commun.*, vol. 13, no. 1, May 2022, Art. no. 2586.

[8] H. Zhang et al., "Topological rainbow based on graded topological photonic crystals," *Opt. Lett.*, vol. 46, no. 6, pp. 1237–1240, Mar. 2021.

[9] H. Yuan, Z. Liu, M. Wei, H. Lin, X. Hu, and C. Lu, "Topological nanophotonic wavelength router based on topology optimization," *Micromachines*, vol. 12, no. 12, Dec. 2021, Art. no. 1506.

[10] C. Lu, H. Wang, J. Miao, W. Guo, X. Xiang, and Y. Liu, "A tunable on-chip integrated plasmonic filter and router based on metal/dielectric nanostructures," *Plasmonics*, vol. 13, no. 1, pp. 115–121, Feb. 2018.

[11] H. Yuan et al., "On-chip cascaded bandpass filter and wavelength router using an intelligent algorithm," *IEEE Photon. J.*, vol. 13, no. 4, Aug. 2021, Art. no. 6600408.

[12] G. Calò and V. Petruzzelli, "Wavelength routers for optical networks-on-chip using optimized photonic crystal ring resonators," *IEEE Photon. J.*, vol. 5, no. 3, Jun. 2013, Art. no. 7901011.

[13] P. B. Deotare, L. C. Kogos, I. Bulu, and M. Lončar, "Photonic crystal nanobeam cavities for tunable filter and router applications," *IEEE J. Sel. Topics Quantum Electron.*, vol. 19, no. 2, Mar./Apr. 2013, Art. no. 3600210.

[14] T. Sridarshini and S. I. Gandhi, "Compact 3×3 wavelength routing for photonic integrated circuits," *Photonic Netw. Commun.*, vol. 36, no. 1, pp. 68–81, Aug. 2018.

[15] L. H. Wu and X. Hu, "Scheme for achieving a topological photonic crystal by using dielectric material," *Phys. Rev. Lett.*, vol. 114, no. 22, Jun. 2015, Art. no. 223901.

[16] X.-T. He et al., "A silicon-on-insulator slab for topological valley transport," *Nature Commun.*, vol. 10, Feb. 2019, Art. no. 872.

[17] F. Gao et al., "Topologically protected refraction of robust kink states in valley photonic crystals," *Nature Phys.*, vol. 14, no. 2, pp. 140–144, Feb. 2018.

[18] Z. Gao et al., "Valley surface-wave photonic crystal and its bulk/edge transport," *Phys. Rev. B*, vol. 96, no. 20, Nov. 2017, Art. no. 201402.

[19] J. Noh, S. Huang, K. P. Chen, and M. C. Rechtsman, "Observation of photonic topological valley hall edge states," *Phys. Rev. Lett.*, vol. 120, no. 6, Feb. 2018, Art. no. 063902.

[20] L. Yuan, Q. Lin, M. Xiao, and S. Fan, "Synthetic dimension in photonics," *Optica*, vol. 5, no. 11, pp. 1396–1405, Nov. 2018.

[21] T. Ozawa and H. M. Price, "Topological quantum matter in synthetic dimensions," *Nature Rev. Phys.*, vol. 1, no. 5, pp. 349–357, May 2019.

[22] A. Dutt, Q. Lin, L. Yuan, M. Minkov, M. Xiao, and S. Fan, "A single photonic cavity with two independent physical synthetic dimensions," *Science*, vol. 367, no. 6473, pp. 59–64, Jan. 2020.

[23] J. Zak, "Berry's phase for energy bands in solids," *Phys. Rev. Lett.*, vol. 62, no. 23, pp. 2747–2750, Jun. 1989.

[24] Y. Nakata, Y. Ito, Y. Nakamura, and R. Shindou, "Topological boundary modes from translational deformations," *Phys. Rev. Lett.*, vol. 124, no. 7, Feb. 2020, Art. no. 073901.

[25] M. I. Shalaev, W. Walasik, A. Tsukernik, Y. Xu, and N. M. Litchinitser, "Robust topologically protected transport in photonic crystals at telecommunication wavelengths," *Nature Nanotechnol.*, vol. 14, no. 1, pp. 31–34, Jan. 2019.

[26] M. Augustin et al., "Highly efficient waveguide bends in photonic crystal with a low in-plane index contrast," *Opt. Exp.*, vol. 11, no. 24, pp. 3284–3289, Dec. 2003.

[27] J. S. Jensen, O. Sigmund, L. H. Frandsen, P. I. Borel, A. Harpoth, and M. Kristensen, "Topology design and fabrication of an efficient double 90/spl deg/photonic crystal waveguide bend," *IEEE Photon. Technol. Lett.*, vol. 17, no. 6, pp. 1202–1204, Jun. 2005.

[28] E. Chow, S. Y. Lin, J. R. Wendt, S. G. Johnson, and J. D. Joannopoulos, "Quantitative analysis of bending efficiency in photonic-crystal waveguide bends at $\lambda = 1.55 \mu m$ wavelengths," *Opt. Lett.*, vol. 26, no. 5, pp. 286–288, Mar. 2001.

[29] M. Askari, B. Momeni, M. Soltani, and A. Adibi, "Systematic design of wide-bandwidth photonic crystal waveguide bends with high transmission and low dispersion," *J. Lightw. Technol.*, vol. 28, no. 11, pp. 1707–1713, Jun. 2010.

[30] G. Arregui, J. Gomis-Bresco, C. M. Sotomayor-Torres, and P. D. Garcia, "Quantifying the robustness of topological slow light," *Phys. Rev. Lett.*, vol. 126, no. 2, Jan. 2021, Art. no. 027403.

[31] R. Sarkissian and J. O'Brien, "Group index oscillations in photonic crystal waveguides," *Appl. Phys. Lett.*, vol. 105, no. 12, Sep. 2014, Art. no. 121102.

[32] C. M. Patil et al., "Observation of slow light in glide-symmetric photonic-crystal waveguides," *Opt. Exp.*, vol. 30, no. 8, pp. 12565–12575, Apr. 2022.

[33] Z. Liu, Y. Zhang, G. Weixuan, Y.-C. Liu, X. Hu, and C. Lu, "Ultrasmall broadband wavelength and polarization router based on hybrid waveguide of monolithic-LiNbO3," *Opt. Lett.*, vol. 44, no. 23, pp. 5772–5775, Dec. 2019.